PHYSICAL REVIEW B **77**, 174412 (2008)

Raman scattering in a Heisenberg $S=\frac{1}{2}$ antiferromagnet on the triangular lattice

Natalia Perkins[1,2] and Wolfram Brenig[2]
[1]*Department of Physics, University of Wisconsin–Madison, Madison, Wisconsin 53706, USA*
[2]*Institute for Theoretical Physics, Technical University Braunschweig, Mendelssohnstrasse 3, 38106 Braunschweig, Germany*
(Received 2 March 2008; published 8 May 2008)

We investigate the two-magnon Raman scattering from the $S=\frac{1}{2}$ Heisenberg antiferromagnet on the triangular lattice by considering both the effect of the renormalization of the one-magnon spectrum by $1/S$ corrections and the final-state magnon-magnon interactions. The bare Raman intensity displays two peaks related to one-magnon Van Hove singularities. We find that $1/S$ self-energy corrections to the one-magnon spectrum strongly modify this intensity profile. The central Raman peak is significantly enhanced due to plateaus in the magnon dispersion, the high frequency peak is suppressed due to magnon damping, and the overall spectral support narrows considerably. Additionally, we investigate final-state interactions by solving the Bethe-Salpeter equation to $O(1/S)$. In contrast to collinear antiferromagnets, the noncollinear nature of the magnetic ground state leads to an irreducible magnon scattering that is retarded and nonseparable already for the lowest order. We show that final-state interactions lead to a rather broad Raman continuum centered on approximately twice the "roton" energy. We also discuss the dependence on the scattering geometry.

DOI: 10.1103/PhysRevB.77.174412 PACS number(s): 78.30.−j

I. INTRODUCTION

Raman scattering is an effective tool to study the excitation spectrum of magnetic systems since the intensity of the inelastically scattered light is directly related to the density of singlet states at zero momentum. In local-moment magnets with well defined magnon excitations, this quantity is linked to the two-magnon density of states. Therefore, magnetic Raman scattering plays an important role in understanding the dynamics and interactions of magnons in conventional spin systems.[1–4] This is particularly true for the spin-1/2 square-lattice Heisenberg antiferromagnet (HAF) of high-T_c superconductor parent compounds, wherein experimental[5–7] and theoretical[8–11] studies of the magnetic correlations by Raman scattering may provide important insights into the energy scales relevant to the pairing mechanism (for reviews, see Refs. 12 and 13).

The Raman scattering from HAFs can be understood in terms of the Loudon-Fleury (LF) processes,[14] in which two magnons are simultaneously created by light absorption and emission. In the limit of large on-site Coulomb correlations U, the Hamiltonian that describe these processes can be obtained as a leading term of the expansion in $t/(U-\omega)$, where t is the nearest-neighbor (NN) hopping and ω is on the order of photon frequencies.[15]

The Raman intensity of HAFs on hypercubic lattices with unfrustrated NN exchange and collinear type of antiferromagnetic (AFM) order allows for a straightforward semiquantitative interpretation in terms of the LF processes. In fact, in real space, exchanging two NN spins of $S=\frac{1}{2}$ leads to an excitation with an energy $\Omega\sim(z-1)J$, where z is the coordination number and J is the AFM exchange energy. The reduction in Ω/J by -1 is a consequence of the exchange link between the NN sites and can be interpreted in terms of a two-magnon interactions in the final state. In momentum space, the linear spin-wave theory yields nondispersive magnons along the magnetic Brillouin zone (BZ) boundary, leading to a square-root divergence of the bare two-magnon density of states at $\Omega=zJ$. Inclusion of the final state magnon-magnon interactions broadens the singularity and shifts it down to $\Omega\sim 2.9J$ (Refs. 8–11) in two dimensions, which is consistent with both the real-space result $\Omega=J(4-1)=3J$ and the experimentally observed Raman profile.

In contrast to conventional collinear HAFs, very little is theoretically known about the Raman scattering from frustrated HAFs. This is intriguing since the singlet spectrum is believed to be an essential fingerprint of such magnets. The spin $S=\frac{1}{2}$ on the triangular Heisenberg antiferromagnet (THAF) lattice with NN exchange interactions is a prominent example of strongly frustrated spin systems. It has a ground state with a noncollinear 120° degree ordering of the spins. Due to this noncollinearity of the classical ground state, nontrivial corrections to the spin-wave spectrum appear already to the first order in $1/S$. It has been shown in Refs. 16–18 that $1/S$ corrections strongly modify the form of the magnon dispersion of the triangular HAF. The resulting dispersion turns out to be almost flat in a wide range of momenta in which it possesses shallow local minima, "rotons," namely, at the midpoint of the faces of the hexagonal BZ. This strongly differs from the classical spin-wave spectrum, which lacks such minima and flat zones. Similar results have been obtained in series expansion studies.[19]

Motivated by these recent findings, in this paper, we analyze the Raman scattering from the THAF by $1/S$ expansion. This is complementary to the recent analysis of Raman scattering on finite, 16 site THAFs by means of exact diagonalization.[20] First, our results show that the Raman intensity is very sensitive to both the $1/S$ corrections of the magnon spectrum and the magnon-magnon interactions in the final state. Moreover, we find that the Loudon-Fleury process on the THAF leads to a Raman profile, which is independent at $O(1/S)$ of the scattering geometry.

The paper is organized as follows: In Sec. II, we review results from existing calculations[16,17] of the one-magnon excitations in the THAF to the first order in $1/S$ that are needed for our study of the Raman spectra. In Sec. III, we consider

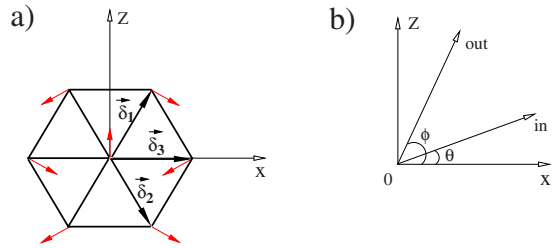

FIG. 1. (Color online) (a) Classical 120° noncollinear spin order on the triangular lattice. Basic vectors of triangular lattice: $\vec{\delta}_1=(1/2,\sqrt{3}/2)$, $\vec{\delta}_2=(1/2,-\sqrt{3}/2)$, and $\vec{\delta}_3=(1,0)$. (b) Definition of scattering angles for the LF vertex.

the LF process to the leading order in $1/S$. In Sec. IV, we calculate the Raman spectrum on various levels of approximation in $1/S$, i.e., bare, one-magnon renormalized, and including final state interactions, and show that the Raman profile is very sensitive to the magnon-magnon interactions. We discuss our results in Sec. V.

II. MODEL

The Hamiltonian of the THAF reads

$$H = J\sum_{\langle ij\rangle} \mathbf{S}_i\mathbf{S}_j, \tag{1}$$

where $\mathbf{S}_i$ are spin-1/2 operators, i refers to sites on the triangular lattice, $\langle\cdot\rangle$ denotes NN summation, and J is the exchange interaction. The classical ground state of the THAF[21] is a noncollinear 120° ordering of spins, which is shown in Fig. 1(a). To avoid the complexity of a three-sublattice notation, it is convenient to work within a locally rotated frame of reference in which the magnetic order is ferromagnetic. To achieve this, we assume a gauge in which the (x,z) coordinates label the lattice plane and a uniform twist with a pitch vector $\mathbf{Q}=(4\pi/3,0)$ is applied to the y axis. The laboratory frame-of-reference spin $\mathbf{S}_i$ is related to the spin $\tilde{\mathbf{S}}_i$ in the rotated frame through

$$\mathbf{S}_i = \begin{bmatrix} \sin(q_i) & -\cos(q_i) & 0 \\ 0 & 0 & -1 \\ \cos(q_i) & \sin(q_i) & 0 \end{bmatrix}^{-1} \tilde{\mathbf{S}}_i, \tag{2}$$

where $q_i=2\pi(2l_i+m_i)/3$ and (l_i,m_i) are integers that label the points on the triangular lattice, which is depicted in Fig. 1(a). In contrast to $\mathbf{S}_i$, the spin $\tilde{\mathbf{S}}_i$ is amenable to a representation in terms of a *single* Holstein-Primakoff boson field on all sites,

$$\tilde{S}_i^z = S - a_i^+a_i,$$

$$\tilde{S}_i^+ = (2S - a_i^+a_i)^{1/2}a_i,$$

$$\tilde{S}_i^- = a_i^+(2S - a_i^+a_i)^{1/2}. \tag{3}$$

Because we intend to study magnon interactions of the first order in $1/S$, we need to expand the Hamiltonian in Eq. (1) up to the quartic order in the boson fields. We have

$$H - E_0 = 3JS(H_2 + H_3 + H_4), \tag{4}$$

where $E_0=3JS^2/2$ is the classical ground state energy and

$$H_2 = \sum_{\mathbf{k}} A_{\mathbf{k}}a_{\mathbf{k}}^\dagger a_{\mathbf{k}} + \frac{B_{\mathbf{k}}}{2}(a_{\mathbf{k}}^\dagger a_{-\mathbf{k}}^\dagger + a_{\mathbf{k}}a_{-\mathbf{k}}), \tag{5}$$

$$H_3 = -i\sqrt{\frac{3}{8S}}\sum_{\mathbf{k}_1,\mathbf{k}_2,\mathbf{k}_3}(a_{\mathbf{k}_1}^\dagger a_{\mathbf{k}_2}^\dagger a_{\mathbf{k}_3} - a_{\mathbf{k}_3}^\dagger a_{\mathbf{k}_2}a_{\mathbf{k}_1}) \times(\bar{\nu}_{\mathbf{k}_1} + \bar{\nu}_{\mathbf{k}_2})\delta_{\mathbf{k}_3,\mathbf{k}_1+\mathbf{k}_2}, \tag{6}$$

$$H_4 = -\frac{1}{16S}\sum_{\mathbf{k}_1,\mathbf{k}_2,\mathbf{k}_3,\mathbf{k}_4}\delta_{\mathbf{k}_3+\mathbf{k}_4,\mathbf{k}_1+\mathbf{k}_2}a_{\mathbf{k}_1}^\dagger a_{\mathbf{k}_2}^\dagger a_{\mathbf{k}_3}a_{\mathbf{k}_4} \times[4(\nu_{\mathbf{k}_1-\mathbf{k}_3} + \nu_{\mathbf{k}_2-\mathbf{k}_3}) + \nu_{\mathbf{k}_1} + \nu_{\mathbf{k}_2} + \nu_{\mathbf{k}_3} + \nu_{\mathbf{k}_4}] - 2\delta_{\mathbf{k}_1+\mathbf{k}_2+\mathbf{k}_3,\mathbf{k}_4}(a_{\mathbf{k}_1}^\dagger a_{\mathbf{k}_2}^\dagger a_{\mathbf{k}_3}^\dagger a_{\mathbf{k}_4} + a_{\mathbf{k}_4}^\dagger a_{\mathbf{k}_3}a_{\mathbf{k}_2}a_{\mathbf{k}_1}) \times(\nu_{\mathbf{k}_1} + \nu_{\mathbf{k}_2} + \nu_{\mathbf{k}_3}), \tag{7}$$

where the momentum $\mathbf{k}$ is defined in the first magnetic BZ. We use the following notations:

$$A_{\mathbf{k}} = 1 + \nu_{\mathbf{k}}/2, \quad B_{\mathbf{k}} = -3\nu_{\mathbf{k}}/2, \tag{8}$$

and the momentum dependent functions are

$$\nu_{\mathbf{k}} = \frac{1}{3}\left(\cos k_x + 2\cos\frac{k_x}{2}\cos\frac{k_y\sqrt{3}}{2}\right), \tag{9}$$

$$\bar{\nu}_{\mathbf{k}} = \frac{2}{3}\sin\frac{k_x}{2}\left(\cos k_x - \cos\frac{k_y\sqrt{3}}{2}\right). \tag{10}$$

The expressions for H_3 and H_4 were first obtained in Ref. 16. The essential difference between Eqs. (4)–(7) and a corresponding expansion around a Neél state on a hypercubic lattice is the occurrence of the term H_3, which is present due to the noncollinearity of the classical ground state configuration of the THAF. In the remainder of this paper, we set the scale of energy to $3J/2=1$, i.e., for $S=\frac{1}{2}$, the prefactor in Eq. (4) is unity.

To proceed, we diagonalize the quadratic part of the Hamiltonian H_2 by a Bogoliubov transformation to a set of magnon quasiparticles,

$$a_{\mathbf{k}} = u_{\mathbf{k}}c_{\mathbf{k}} + v_{\mathbf{k}}c_{-\mathbf{k}}^\dagger,$$

$$a_{\mathbf{k}}^\dagger = u_{\mathbf{k}}c_{\mathbf{k}}^\dagger + v_{\mathbf{k}}c_{-\mathbf{k}}, \tag{11}$$

where $c_{\mathbf{k}}^{(\dagger)}$ are bosons and the coherence coefficients,

$$u_{\mathbf{k}} = \sqrt{\frac{A_{\mathbf{k}} + E_{\mathbf{k}}}{2E_{\mathbf{k}}}},$$

$$v_{\mathbf{k}} = -\frac{B_{\mathbf{k}}}{|B_{\mathbf{k}}|}\sqrt{\frac{A_{\mathbf{k}} - E_{\mathbf{k}}}{2E_{\mathbf{k}}}}, \tag{12}$$

satisfy $u_{\mathbf{k}}^2 - v_{\mathbf{k}}^2 = 1$. The Hamitonian H_2 in terms of the Bogoliubov quasiparticles reads

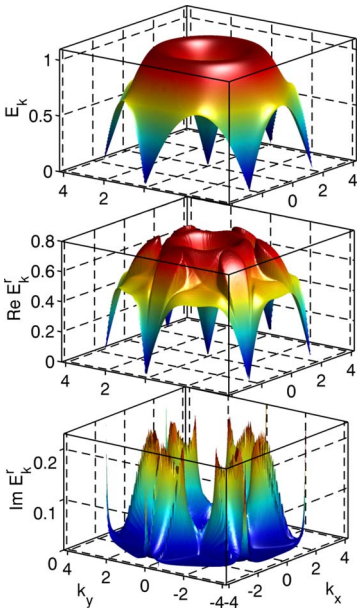

FIG. 2. (Color online) One magnon dispersion. Top: Linear spin-wave dispersion $E_{\mathbf{k}}$ from Eq. (14). Middle and bottom: Real and imaginary parts Re(Im)$E^r_{\mathbf{k}}$ of one magnon dispersion to $O(1/S)$ from a solution of Eqs. (10)–(12) of Ref. 17 on a lattice of 252 $\times 252$ $\mathbf{k}$ points with artificial line broadening of $\eta=0.05$.

$$H_2 = \sum_{\mathbf{k}} E_{\mathbf{k}} c^\dagger_{\mathbf{k}} c_{\mathbf{k}}, \tag{13}$$

and the dispersion is given by

$$E_{\mathbf{k}} = \sqrt{A^2_{\mathbf{k}} - B^2_{\mathbf{k}}} = \sqrt{(1-\nu_{\mathbf{k}})(1+2\nu_{\mathbf{k}})}. \tag{14}$$

The magnon dispersion $E_{\mathbf{k}}$ is depicted in Fig. 2. It vanishes at the center of the zone, $k_x=0$, $k_y=0$, where $\nu_{\mathbf{k}}=1$ and at the corners of the BZ, where $\nu_k=-1/2$. There are two Van Hove singularities, i.e., at $E=3/(2\sqrt{2})\simeq 1.061$ from the maximum energy and at $E=2/3\simeq 0.6667J$ from the zone boundary.

To treat the interaction between magnons, we need to express the triplic and quartic parts of the Hamiltonian, H_3 and H_4, in terms of the quasiparticles $c^{(\dagger)}_{\mathbf{k}}$ by using the transformation of Eq. (11). For the triplic part, we obtain

$$H_3 = \sum_{\mathbf{k},\mathbf{p}} [c_{\mathbf{k}} c^\dagger_{\mathbf{p}} c^\dagger_{\mathbf{k}-\mathbf{p}} f(\mathbf{k},\mathbf{p}) + c_{\mathbf{k}} c^\dagger_{\mathbf{p}} c_{-\mathbf{k}+\mathbf{p}} g(\mathbf{k},\mathbf{p}) + O(c^\dagger c^\dagger c^\dagger + \text{H.c.})]. \tag{15}$$

Terms with three creation (destruction) operators are present in principle but are not explicitly expressed for notational simplicity. As will become clear in Sec. IV, they play no role in evaluating the magnon interactions within the Raman response. Moreover,

$$f(\mathbf{k},\mathbf{p}) = i\sqrt{3}[\bar{\nu}_{\mathbf{p}}(u_{\mathbf{k}}u_{\mathbf{k}-\mathbf{p}} + v_{\mathbf{k}}v_{\mathbf{k}-\mathbf{p}})(u_{\mathbf{p}} + v_{\mathbf{p}}) - \bar{\nu}_{\mathbf{k}}(u_{\mathbf{k}} + v_{\mathbf{k}}) \times (u_{\mathbf{p}}v_{\mathbf{k}-\mathbf{p}} + u_{\mathbf{k}-\mathbf{p}}v_{\mathbf{p}}) + \bar{\nu}_{\mathbf{k}-\mathbf{p}}(u_{\mathbf{k}-\mathbf{p}} + v_{\mathbf{k}-\mathbf{p}}) \times (u_{\mathbf{k}}u_{\mathbf{p}} + v_{\mathbf{k}}v_{\mathbf{p}})], \tag{16}$$

$$g(\mathbf{k},\mathbf{p}) = i\sqrt{3}[\bar{\nu}_{\mathbf{p}}(u_{\mathbf{k}-\mathbf{p}}v_{\mathbf{k}} + u_{\mathbf{k}}v_{\mathbf{k}-\mathbf{p}})(u_{\mathbf{p}} + v_{\mathbf{p}}) + \bar{\nu}_{\mathbf{k}-\mathbf{p}}(u_{\mathbf{k}-\mathbf{p}} + v_{\mathbf{k}-\mathbf{p}})(u_{\mathbf{k}}u_{\mathbf{p}} + v_{\mathbf{k}}v_{\mathbf{p}}) - \bar{\nu}_{\mathbf{k}}(u_{\mathbf{k}} + v_{\mathbf{k}}) \times (u_{\mathbf{k}-\mathbf{p}}u_{\mathbf{p}} + v_{\mathbf{k}-\mathbf{p}}v_{\mathbf{p}})]. \tag{17}$$

For the quartic part, we obtain

$$H_4 = -\frac{1}{16S}\sum_{\mathbf{k},\mathbf{p}} h(\mathbf{k},\mathbf{p}) c_{\mathbf{k}} c_{-\mathbf{k}} c^\dagger_{\mathbf{p}} c^\dagger_{-\mathbf{p}} + O(c^\dagger c^\dagger c^\dagger c^\dagger + c^\dagger c^\dagger c^\dagger c + \text{H.c.}), \tag{18}$$

where, again, terms irrelevant for the Raman scattering are not explicitly displayed, and

$$h(\mathbf{k},\mathbf{p}) = 2((u^2_{\mathbf{k}}u^2_{\mathbf{p}} + v^2_{\mathbf{k}}v^2_{\mathbf{p}})(\nu_{\mathbf{k}} + 4\nu_{\mathbf{k}-\mathbf{p}} + \nu_{\mathbf{p}}) - 3(u^2_{\mathbf{k}} + v^2_{\mathbf{k}})u_{\mathbf{p}}v_{\mathbf{p}}(2\nu_{\mathbf{k}} + \nu_{\mathbf{p}}) - 3(u^2_{\mathbf{p}} + v^2_{\mathbf{p}})u_{\mathbf{k}}v_{\mathbf{k}}(\nu_{\mathbf{k}} + 2\nu_{\mathbf{p}}) + 4u_{\mathbf{k}}v_{\mathbf{k}}u_{\mathbf{p}}v_{\mathbf{p}}(2 + \nu_{\mathbf{k}} + \nu_{\mathbf{p}} + 2\nu_{\mathbf{k}+\mathbf{p}})). \tag{19}$$

Equations (15)–(19) allow us to construct all vertices relevant to the final state two-magnon interactions in the Raman scattering. Apart from that, Eqs. (4)–(10) can be used to derive the one-magnon self-energy to $O(1/S)$. This was done in Ref. 16, to which we refer the reader for details. For the purpose of the present work, it is sufficient to employ Eqs. (10)–(12) of Ref. 16 to calculate the renormalized magnon dispersion $E^r_{\mathbf{k}}$ to $O(1/S)$. Figure 2 (middle and bottom panels) shows the result of such calculations. It is evident that in the real part of the magnon energy, the interactions lead to extended and almost flat regions with a shallow rotonlike minimum along the BZ faces. Moreover, as the Im $E^r_{\mathbf{k}}$ almost vanishes at these regions, the lifetime of a quasiparticle with corresponding momenta is very large. On the other hand, quasiparticles with near-maximum energies are located in the momentum regions of rather large damping.

III. LOUDON-FLEURY VERTEX

We use the framework of the LF model for the interaction of light with spin degrees of freedom for the calculation of the two-magnon Raman scattering. The LF vertex has the form

$$R = \sum_{i\delta} (\hat{\varepsilon}_{\text{in}} \cdot \delta)(\hat{\varepsilon}_{\text{out}} \cdot \delta)\tilde{\mathbf{S}}_i \tilde{\mathbf{S}}_{i+\delta}, \tag{20}$$

where the polarizations $\hat{\varepsilon}_{\text{in}}=\cos\theta\hat{x}+\sin\theta\hat{y}$ and $\hat{\varepsilon}_{\text{out}}=\cos\phi\hat{x}+\sin\phi\hat{y}$ of the incoming and the outgoing light are determined by the angles θ and ϕ, which are defined with respect to the x axis. To derive the final form of the scattering LF vertex, we first write the spin operators in terms of the Holstein-Primakoff bosonic a operators [Eq. (3)] and then express the latter in terms of the boson quasiparticle operators c. We get the following expression:

$$R = \sum\nolimits_k M_{\mathbf{k}}(c_{\mathbf{k}}c_{-\mathbf{k}} + c^\dagger_{\mathbf{k}}c^\dagger_{-\mathbf{k}}) \equiv r^- + r^+, \tag{21}$$

where $M_{\mathbf{k}}$ is given by

$$M_{\mathbf{k}} = [F_1(\theta,\phi) + F_2(\mathbf{k},\theta,\phi)]u_{\mathbf{k}}v_{\mathbf{k}} - \tfrac{3}{4}F_2(\mathbf{k},\theta,\phi)(u^2_{\mathbf{k}} + v^2_{\mathbf{k}}), \tag{22}$$

and we have introduced the following notations:

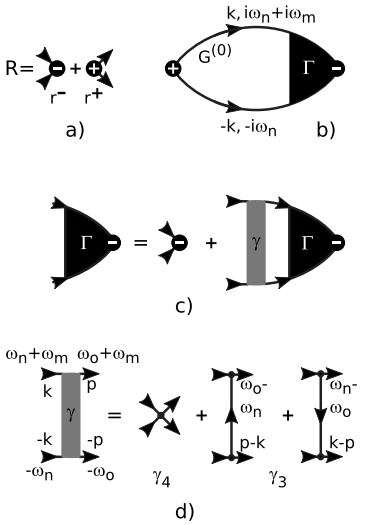

FIG. 3. Diagrams for the Raman intensity: (a) bare Raman vertex R from Eq. (21); (b) Raman susceptibility [both bare, G^0, and dressed, G, magnon propagators are considered (see text)]. (c) The integral equation for the dressed Raman vertex Γ in terms of the irreducible magnon particle-particle (IPP) vertex γ. (d) Leading order $1/S$ contributions to the IPP vertex.

$$F_1(\theta,\phi) = 2S\sum_{\mu=1}^{3} f_\mu(\theta,\phi),$$

$$F_2(\mathbf{k},\theta,\phi) = 2S\left[f_3(\theta,\phi)\cos k_x + f_1(\theta,\phi)\cos\left(\frac{k_x}{2}+\frac{\sqrt{3}}{2}k_y\right)\right.$$
$$\left. + f_2(\theta,\phi)\cos\left(\frac{k_x}{2}-\frac{\sqrt{3}}{2}k_y\right)\right],$$

$$f_\mu(\theta,\phi) = \hat{\varepsilon}_{\text{in}}\cdot\delta_\mu. \tag{23}$$

In principle, the Raman vertex contains also $c_{\mathbf{k}}^\dagger c_{\mathbf{k}}$ terms. However, at zero momentum and for the lowest order in $1/S$, these terms do not contribute to the Raman response at finite frequency, and we dropped them. Note that R is explicitly Hermitian.

IV. RAMAN INTENSITY

We now calculate the Raman intensity including the one- and two-magnon renormalizations up to $O(1/S)$. The Raman intensity $I(\Omega)$ is obtained via Fermi's golden rule from

$$I(\omega_m) = \text{const} \times \text{Im}\left[\int_0^\beta d\tau e^{i\omega_m\tau}\langle T_\tau[R(\tau)R]\rangle\right] \tag{24}$$

by analytic continuation of the bosonic Matsubara frequencies $\omega_m = 2\pi mT$ onto the real axis as $i\omega_m \to \Omega + i\eta$, where $\Omega = \omega_{\text{in}} - \omega_{\text{out}}$, which refers to the inelastic energy transfer by the photon; for the remainder of this paper, we assume the temperature $T = 1/\beta$ to be zero. The prefactor "const" refers to some arbitrary units by which the observed intensities are scaled.

The role of the interactions is summarized in Fig. 3. Two effects have to be distinguished, namely, renormalizations of the one-magnon propagators, i.e., $G^0 \to G$, and vertex corrections to the Raman intensity (final state interactions), i.e., $R \to \Gamma$.

All propagators are expressed in $c_k^{(\dagger)}$-type terms of the Bogoliubov particles. For orders higher than $O[(1/S)^0]$, the propagators of these particles are not diagonal, i.e., both normal $G_{cc}(\mathbf{k},\tau) = -\langle T_\tau(c_{\mathbf{k}}(\tau)c_{\mathbf{k}}^\dagger)\rangle$ and anomalous $D_{cc}(\mathbf{k},\tau) = -\langle T_\tau[c_{\mathbf{k}}(\tau)c_{-\mathbf{k}}]\rangle$ propagators do occur. However, anomalous propagators are smaller by one factor of $1/S$ as compared to the normal propagators and therefore can be neglected. For the first order in $1/S$, the normal propagators read $G(\mathbf{k}, i\omega_n) = 1/(i\omega_n - E_{\mathbf{k}}^r)$, i.e., the quasiparticle residue remains unity, and $E_{\mathbf{k}}^r$ is taken from Eqs. (10)–(12) of Ref. 17.

In order to evaluate the Raman intensity [Eq. (24)], we have to calculate the Raman susceptibility $\langle T_\tau[R(\tau)R]\rangle$. In principle, the latter can contain terms of type $\langle T_\tau[r^-(\tau)r^-]\rangle$, with $r^\pm$ specified in Eq. (21) and Fig. 3(a). However, these terms need at least one $O(1/S)$ interaction event to occur or require anomalous propagators, i.e., they are smaller by one order of $1/S$ and will be dropped. In the following, we consider only $\langle T_\tau[r^+(\tau)r^-]\rangle + \langle T_\tau[r^-(\tau)r^+]\rangle$. By Hermitian conjugation, it is sufficient to calculate $J(\tau) = \langle T_\tau[r^-(\tau)r^+]\rangle$, which is depicted in Fig. 3(b).

Figure 3(b) shows the two-particle reducible Raman vertex $\Gamma(\mathbf{k},\omega_n,\omega_m)$, which includes a series of magnon-magnon interaction events. It satisfies the Bethe-Salpeter equation expressed in terms of the two-particle irreducible vertex γ, which is depicted in Fig. 3(c),

$$\Gamma(\mathbf{k},\omega_n,\omega_m) = r^-(\mathbf{k}) + \sum_{\mathbf{p},\omega_o}\gamma(\mathbf{k},\mathbf{p},\omega_n,\omega_o)G(\mathbf{p},\omega_o+\omega_m)$$
$$\times G(-\mathbf{p},-\omega_o)\Gamma(\mathbf{p},\omega_o,\omega_m). \tag{25}$$

In this work, we consider only the leading order contributions in $1/S$ to γ. They are shown in Fig. 3(d). The quartic vertex $\gamma_4(\mathbf{k},\mathbf{p})$ is identical to the two-particle-two-hole contribution from H_4 of Eqs. (18) and (19) and reads

$$\gamma_4(\mathbf{k},\mathbf{p}) = -\frac{1}{2S}h(\mathbf{k},\mathbf{p}). \tag{26}$$

The two addends forming the irreducible vertex $\gamma_3(\mathbf{k},\mathbf{p},\omega_n,\omega_o)$ are assembled from H_3 and one intermediate propagator and can be written as

$$\gamma_3(\mathbf{k},\mathbf{p},\omega_n,\omega_o) = \frac{1}{2S}\sum_{\mathbf{k},\mathbf{p}}[f(\mathbf{k},\mathbf{p})g(-\mathbf{k},-\mathbf{p})$$
$$\times G^0(\mathbf{k}-\mathbf{p}, i\omega_o - i\omega_n)$$
$$\times c_{\mathbf{k}}c_{-\mathbf{k}}c_{\mathbf{p}}^\dagger c_{-\mathbf{p}}^\dagger + g(\mathbf{k},\mathbf{p})f(-\mathbf{k},-\mathbf{p})$$
$$\times G^0(\mathbf{p}-\mathbf{k}, i\omega_n - i\omega_o)]c_{\mathbf{k}}c_{-\mathbf{k}}c_{\mathbf{p}}^\dagger c_{-\mathbf{p}}^\dagger, \tag{27}$$

where the functions $f(\mathbf{k},\mathbf{p})$ and $g(\mathbf{k},\mathbf{p})$ obey the symmetry relation $f[g](-\mathbf{k},-\mathbf{q}) = -f[g](\mathbf{k},\mathbf{q})$.

To keep γ_3 to the leading order in $1/S$, we retain only the zeroth order propagators G^0 for each intermediate line. In principle, H_3 allows for an additional two-particle irreducible graph, with the incoming (outgoing) legs placed into the

particle-particle (hole-hole) channel and one intermediate line at zero momentum and frequency. However, we verified that these contributions exactly vanish.

Due to γ_3, Eq. (25) is an integral equation with respect to *both* momentum and frequency. This is the first major difference of the Raman scattering from collinear HAFs, where only γ_4 exists at $O(1/S)$. To proceed, further approximations have to be made. Here, we simplify γ_3 by assuming the dominant contribution from the frequency summations to result from the *mass shell* of the propagators in the intermediate particle-particle reducible sections of Fig. 3(c),

$$-i\omega_n \approx E_{\mathbf{k}},$$

$$-i\omega_o \approx E_{\mathbf{p}}. \tag{28}$$

This approximation will be best for sharp magnon lines and the transferred frequencies $i\omega_m$ close to the Van Hove singularities of $2E_{\mathbf{k}}$.

In this approximation for γ_3, the two-particle irreducible vertex γ simplifies to

$$\gamma(\mathbf{k},\mathbf{p},\omega_n,\omega_o) \approx \gamma(\mathbf{k},\mathbf{p}) = \gamma_3(\mathbf{k},\mathbf{p}) + \gamma_4(\mathbf{k},\mathbf{p})$$
$$= -\frac{1}{2S}\left(\frac{2E_{\mathbf{k}-\mathbf{p}} f(\mathbf{k},\mathbf{p}) g(\mathbf{k},\mathbf{p})}{(E_{\mathbf{k}}-E_{\mathbf{p}})^2 - E_{\mathbf{k}-\mathbf{p}}^2} + h(\mathbf{k},\mathbf{p})\right). \tag{29}$$

Now, we can perform the frequency summation over ω_o on the right hand side of Eq. (25) as well as the analytic continuation $i\omega_m \to \Omega + i\eta \equiv z$. With this, Γ in the latter equation turns into a function of $\mathbf{p}$ and z only, leading to

$$\sum_{\mathbf{p}} L_{\mathbf{k},\mathbf{p}}(z)\Gamma_{\mathbf{p}}(z) = r^{-}(\mathbf{k}), \tag{30}$$

$$L_{\mathbf{k},\mathbf{p}}(z) = \delta_{\mathbf{k},\mathbf{p}} - \frac{\gamma(\mathbf{k},\mathbf{p})}{z - 2E_{\mathbf{p}}^{(r)}}, \tag{31}$$

which is an integral equation with respect to momentum only. In the rest of the paper, the superscript r refers to the case when *renormalized* propagators with $E_{\mathbf{p}}^r$ are taken in the two-particle reducible part of the Raman intensity, while $E_{\mathbf{p}}$ corresponds to the usage of *bare* propagators.

Close inspection of the vertex $\gamma(\mathbf{k},\mathbf{p})$ shows that it does not separate into a *finite* sum of products of lattice harmonics of the triangular lattice. Therefore, Eqs. (30) and (31) cannot be algebraically solved in terms of a finite number of scattering channels but require a numerical solution. On finite lattices, this can be done by treating Eq. (30) as a linear equation for $\Gamma_{\mathbf{p}}(z)$ at fixed z. This marks another significant difference between Raman scattering from collinear and noncollinear antiferromagnets.

Finally, the expression for the Raman intensity from Eq. (24) can be written as

$$I(\Omega) = \text{const} \times [J(\Omega) - J(-\Omega)]. \tag{32}$$

$$J(\Omega) = \text{Im}\left[\sum_{\mathbf{k}} \frac{M_{\mathbf{k}}\Gamma_{\mathbf{k}}(\Omega + i\eta)}{\Omega + i\eta - 2E_{\mathbf{k}}^{(r)}}\right]. \tag{33}$$

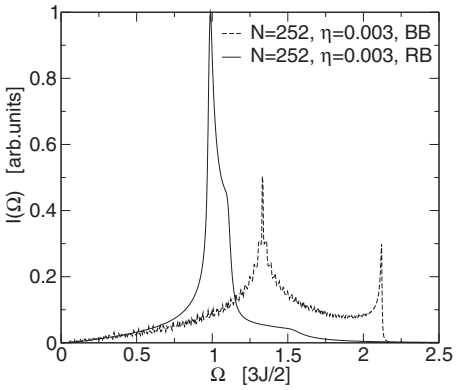

FIG. 4. Raman intensity neglecting final state interactions, i.e., replacing Γ by M in Eq. (33). Scattering geometry: $\phi=\theta=0$. Number of $\mathbf{k}$ points: $N\times N$. Dashed curve (BB): bubble obtained by using bare magnon energies $E_{\mathbf{k}}$ from Eq. (14), as shown in top panel of Fig. 2. The imaginary broadening $\eta=0.003$ was chosen as such as to retain visible but small finite-size oscillations. Solid curve (RB): bubble obtained by using renormalized magnon energies $E_{\mathbf{k}}^r$ to $O(1/S)$ obtained from Eqs. (10)–(12) of Ref. 17 and shown in the middle and lower panels of Fig. 2. Finite-size oscillations are suppressed by $\text{Im}[E_{\mathbf{k}}^r]$. The absolute scale of $I(\Omega)$ is set to unity, but the relative scale of BB and RB is kept.

We now discuss the Raman intensity for several levels of approximations. First, we neglect final state interactions and set $\Gamma_{\mathbf{k}}(z) \to M_{\mathbf{k}}$. Figure 4 shows the Raman intensity as a function of the transferred photon frequencies Ω for this case. Figure 4 contrasts the Raman bubble with the bare propagators against that with the renormalized ones. Such results can be obtained on fairly large lattices since they do not involve a solution of the integral equation (30) but only a calculation of the one magnon self-energy.[17] We keep the shift $i\eta$ off the real axis deliberately small in Fig. 4 in order to discriminate its effect from that of the actual lifetime broadening due to the imaginary part of $E_{\mathbf{k}}^r$.

First, we would like to note that we find the line shape to be *insensitive* to the scattering geometry. This is in a sharp contrast to the Raman scattering from the square lattice HAF, wherein Raman amplitudes in A_{1g}, B_{1g}, and B_{2g} symmetries are very different.

In case of the bare Raman bubble, one can see two well-defined peaks, one at energy $\Omega=3/\sqrt{2}$ and one at $\Omega=4/3$—both in units of $3J/2$. These energies correspond to two times that of the maximum and of the BZ-boundary saddle point of the classical spin-wave spectrum $E_{\mathbf{k}}$. Clearly, the dominant spectral weight does not stem from the $\mathbf{k}$ points at the upper cutoff of the linear spin-wave energy but from the BZ boundary. This does not reflect the bare two-magnon density of states but is an effect of the Raman matrix element $M_{\mathbf{k}}$, which preferentially samples the BZ regions.

Switching on $1/S$ corrections, two modifications of the intensity occur. First, both maxima are shifted downward by a factor of ~ 0.7 due to the corresponding renormalizations of the one magnon energies. Second, as the BZ-boundary saddle point of $E_{\mathbf{k}}$ has turned into a flat region, which occupies substantial parts of the BZ for $E_{\mathbf{k}}^r$, the intensity of the lower energy peak is strongly enhanced due to the very large

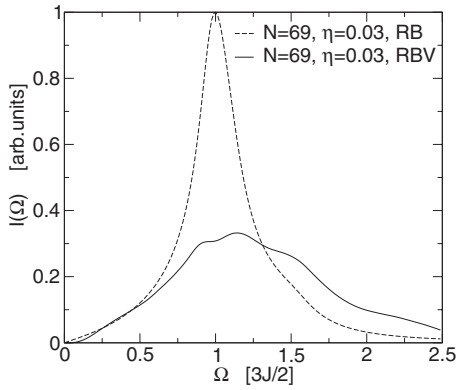

FIG. 5. Effect of final state interactions on Raman intensity. Scattering geometry: $\phi=\theta=0$. Number of $\mathbf{k}$ points: $N\times N$. Imaginary shift off real axis is $\eta=0.03$. Dashed line (RB): replacing Γ by M in Eq. (33) and using bubble with renormalized magnon energies $E^r_{\mathbf{k}}$ to $O(1/S)$ obtained from Eqs. (10)–(12) of Ref. 17. Solid line (RBV): using dressed vertex Γ obtained from Eq. (30) in Eq. (33) and renormalized magnon energies $E^r_{\mathbf{k}}$. The absolute scale of $I(\Omega)$ is set to unity, but the relative scale of RB and RBV is kept.

density of one-magnon states. Equally important, the imaginary part of $E^r_{\mathbf{k}}$ is finite in the BZ region, which corresponds to the maximal one-magnon energies. This almost completely smears the peak at the upper frequency cutoff in $I(\Omega)$, as can be seen from the solid line in Fig. 4. In contrast to that, $\mathrm{Im}[E^r_{\mathbf{k}}]$ almost vanishes in the flat regions on the BZ boundary due to phase-space constraints,[18] leading to a further relative enhancement of the intensity from there.

Next, we turn to final-state interactions. In Fig. 5, we compare $I(\Omega)$ from the Raman bubble obtained with the propagators renormalized to $O(1/S)$ and only bare Raman vertices to the intensity obtained by also including the dressed Raman vertex $\Gamma_{\mathbf{k}}(z)$ from Eq. (30). The numerical solution of the latter equation requires some comments. Since the kernel $L_{\mathbf{k},\mathbf{p}}(z)$ is not sparse and has rank $N^2\times N^2$, already moderate lattice sizes lead to rather large dimensions and storage requirements for the linear solver. We have chosen $N=69$, leading to a 4761×4761 system, which we have solved 200 times to account for 200 frequencies in the interval $\Omega\in[0,2.5]$. The kernel has the points and lines of a singular behavior in the $(\mathbf{k},\mathbf{p})$ space, which stem from the singularities of the Bogoliubov factors $u[v](\mathbf{k})$ in $f[g][h](\mathbf{k},\mathbf{p})$ and from the energy denominators in Eq. (29). In principle, such regions are of measure zero with respect to the complete $(\mathbf{k},\mathbf{p})$ space, yet we have no clear understanding of their impact on a solution of Eq. (30) as $N\to\infty$. In our case, i.e., a finite lattice, we have chosen to regularize these points and lines by cutting off eventual singularities in $L_{\mathbf{k},\mathbf{p}}$. The comparatively small system sizes require a rather larger artificial broadening $i\eta$ in order to achieve acceptably smooth line shapes. This can be seen by contrasting the dashed curve in Fig. 5 and the solid curve in Fig. 4, which correspond to *identical* quantities, however, for different finite systems, 252×252 vs 69×69.

The main message put forward by Fig. 5 is that the final state interactions lead to a flattening of the peak from the two-magnon density of states, transforming it to a rather broad Raman continuum. This can be understood, at least qualitatively, from the RPA-like functional form of the Bethe-Salpeter equation. Discarding momentum dependencies and iterating the two-magnon bubble times, the irreducible vertex γ leads to a renormalization of the intensity by a factor roughly of the form $\sim 1/[1-\gamma\cdot\rho(\Omega)]$, where $\rho(\Omega)$ refers to the two-magnon bubble. Directly at the peak position of the Raman bubble, this renormalization factor may get small, thereby suppressing the overall intensity. While exactly the same mechanism is also at work for the square lattice HAF, its impact on the spectrum is completely different. In the latter case, the peak intensity without final state interactions is at the upper cutoff of the Raman intensity. Suppression of this peak intensity simply shifts the maximum intensity to lower frequencies within the Raman spectrum. This shift is then interpreted in terms of a two-magnon binding energy. Such reasoning cannot be pursued in the present case.

V. CONCLUSION AND DISCUSSION

To summarize, we have investigated the magnetic Raman scattering from the two-dimensional triangular Heisenberg antiferromagnet by considering various levels of approximation within a controlled $1/S$ expansion. Our study has revealed several key differences as compared to the well-known magnetic Raman scattering from the planar square lattice spin-1/2 antiferromagnet.

First, we found that the intensity profile is insensitive to the in-plane scattering geometry of the incoming and outgoing light at $O(1/S)$. This has to be contrasted against the clear difference between A_{1g} and $B_{1g,2g}$ symmetries for the square-lattice case.

Second, on the level of the linear spin-wave theory, we showed that the Raman intensity has two Van Hove singularities. The less intensive peak is located at the upper edge of the two-magnon density of states and stems from twice the maximum of the one-magnon energy. This is similar to the square lattice case. However, the dominant peak is located approximately in the center of the two-magnon density of states. This peak stems from the Loudon-Fleury Raman vertex that strongly selects the Brillouin zone boundary regions where the one-magnon dispersion on the triangular lattice has an additional weak Van Hove singularity. This is absent on the square lattice.

Next, we calculated the Raman intensity with the one-magnon spectrum renormalized to $O(1/S)$ by neglecting, however, the final-state interactions within the Raman process. In this case, we have obtained a sharp and almost δ-functional Raman peak at an energy of $\sim 3J/2$. At this energy, the real part of the renormalized one-magnon dispersion shows a large plateau region at the Brillouin zone boundary with a rotonlike shallow minimum. Moreover, due to phase-space constraints, the one-magnon lifetime is large in this region. Therefore, the two-magnon density of states in this region is strongly enhanced, as compared to the linear spin-wave result. In contrast to that, the intensity at the upper edge of the spectrum is suppressed further since the $O(1/S)$ corrections lead to the significant one-magnon damping. Fi-

nally, the overall width of the spectrum is reduced by a factor of approximately 0.7.

In the last step, we considered the impact of the final-state interactions to $O(1/S)$. Due to the noncollinear ordering on the triangular lattice and in a sharp contrast to the square-lattice case, we find that even to the lowest order, the two-magnon scattering is neither instantaneous in time nor separable in momentum space. Our solution of the corresponding Bethe-Salpeter equation reveals a broad continuumlike Raman profile, which results from a smearing of the intensity of the two-roton peak by virtue of repeated two-magnon scattering. While at this order in $1/S$ the overall form of the Raman profile is reminiscent of that on the square lattice, one has to keep in mind that in the latter case, the position of the maximum in the center of the Raman continuum has to be interpreted rather differently, namely, in terms of a two-magnon binding effect.

In conclusion, we hope that our theoretical investigation will stimulate further experimental analysis of triangular and more generally frustrated magnetic systems by Raman scattering. Several novel materials with triangular structure have been thoroughly investigated over the past few years, among them the cobaltite, Na_xCoO_2,[22] and the spatially anisotropic triangular antiferromagents Cs_2CuCl_4 (Ref. 23) and κ-$(BEDT\text{-}TTF)_2Cu_2(CN)_3$.[24] To our knowledge, however, magnetic Raman scattering on such systems remains a rather open issue.

ACKNOWLEDGMENTS

We would like to thank A. Chubukov for useful discussions. One of us (W.B.) acknowledges partial support by the DFG through Grant No. BR 1084/4-1 and the hospitality of the KITP, where this research was supported in part by the NSF under Grant No. PHY05-51164.

[1] R. J. Elliot and R. Loudon, Phys. Lett. **3A**, 189 (1963).
[2] P. A. Fleury, S. P. S. Porto, L. E. Cheesman, and H. J. Guggenheim, Phys. Rev. Lett. **17**, 84 (1966).
[3] J. B. Parkinson, J. Phys. C **2**, 2012 (1969).
[4] P. A. Fleury and H. J. Guggenheim, Phys. Rev. Lett. **24**, 1346 (1970).
[5] K. B. Lyons, P. A. Fleury, J. P. Remeika, A. S. Cooper, and T. J. Negran, Phys. Rev. B **37**, 2353 (1988).
[6] S. Sugai, S. I. Shamoto, and M. Sato, Phys. Rev. B **38**, 6436 (1988).
[7] P. E. Sulewski, P. A. Fleury, K. B. Lyons, and S.-W. Cheong, Phys. Rev. Lett. **67**, 3864 (1991).
[8] R. R. P. Singh, P. A. Fleury, K. B. Lyons, and P. E. Sulewski, Phys. Rev. Lett. **62**, 2736 (1989).
[9] C. M. Canali and S. M. Girvin, Phys. Rev. B **45**, 7127 (1992).
[10] A. V. Chubukov and D. M. Frenkel, Phys. Rev. Lett. **74**, 3057 (1995).
[11] F. Nori, R. Merlin, S. Haas, A. W. Sandvik, and E. Dagotto, Phys. Rev. Lett. **75**, 553 (1995).
[12] G. Blumberg, M. Kang, M. V. Klein, K. Kadowaki, and C. Kendziora, Science **278**, 1427 (1997).
[13] T. P. Devereaux and R. Hackl, Rev. Mod. Phys. **79**, 175 (2007).
[14] P. A. Fleury and R. Loudon, Phys. Rev. **166**, 514 (1968).
[15] B. S. Shastry and B. I. Shraiman, Phys. Rev. Lett. **65**, 1068 (1990).
[16] A. V. Chubukov, S. Sachdev, and T. Senthil, J. Phys.: Condens. Matter **6**, 8891 (1994).
[17] O. A. Starykh, A. V. Chubukov, and A. G. Abanov, Phys. Rev. B **74**, 180403(R) (2006).
[18] A. L. Chernyshev and M. E. Zhitomirsky, Phys. Rev. Lett. **97**, 207202 (2006).
[19] W. H. Zheng, J. O. Fjaerestad, R. R. P. Singh, R. H. McKenzie, and R. Coldea, Phys. Rev. B **74**, 224420 (2006).
[20] F. Vernay, T. P. Devereaux, and M. J. P. Gingras, J. Phys.: Condens. Matter **19**, 145243 (2007).
[21] T. Jolicoeur and J. C. LeGuillou, Phys. Rev. B **40**, 2727 (1989).
[22] K. Takada, H. Sakurai, E. Takayama-Muromachi, F. Izumi, R. A. Dilanian, and T. Sasaki, Nature (London) **422**, 53 (2003).
[23] R. Coldea, D. A. Tennant, K. Habicht, P. Smeibidl, C. Wolters, and Z. Tylczynski, Phys. Rev. Lett. **88**, 137203 (2002).
[24] Y. Shimizu, K. Miyagawa, K. Kanoda, M. Maesato, and G. Saito, Phys. Rev. Lett. **91**, 107001 (2003).